Volume 1 | Number 1 | Jan 2013 | Pages 1–100

Journal of
Materials Chemistry A

Materials for energy and sustainability
www.rsc.org/materialsA

Li⁺

ROYAL SOCIETY
OF CHEMISTRY

ROYAL SOCIETY
OF **CHEMISTRY**

www.rsc.org/materialsA

Journal Name

Dynamic Article Links ▶

ARTICLE TYPE

New Mesoporous Titanosilicate MCM-36 Material Synthesized by Pillaring Layered ERB-1 Precursor

Fang Jin,[1,2] Chih-Cheng Chang,[1] Ciao-Wei Yang,[1] Jyh–Fu Lee,[3] Ling–Yun Jang,[3] and Soofin Cheng[1]*

A new Ti-containing MCM-36 material (abbreviated Si/Ti-MCM-36(E)) was prepared through a sequential step started with the ERB-1 precursor, which was a borosilicate and aluminum-free analogue 10 of MCM-22 precursor owning the MWW layer structure. The layered precursors were swollen with hexadecyltrimethylammonium bromide and tetrapropylammonium hydroxide, followed by pillaring the sheets with titanosilicate formed via hydrolysis of interlayer tetraethylorthosilicate and tetrabutylorthotitanate. In comparison with MCM-22, ERB-1 precursor was more effective in forming ordered stacking structure and generating 2 nm mesopores, and the resultant Si/Ti-MCM-36(E) was of 15 lower acidity. The Ti *K*-edge X-ray absorption spectra indicated that Ti could be well distributed in Si/Ti-MCM-36(E) without formation of TiO_2 clusters through control of the Si/Ti ratio in pillaring. The subsequent acid treatment would remove mainly octahedrally coordinated Ti and left tetrahedrally coordinated Ti species as the active centers in catalytic epoxidation of cyclohexene. Acid treatment further decreased the acidity of the sample and enhanced the surface hydrophobicity. In comparison with 20 microporous Ti-YNU-1, Ti-MWW and TS-1, the 2 nm mesopores in Si/Ti-MCM-36(E) effectively improved the accessibility of bulky molecules to the active Ti sites, and surface hydrophobicity significantly enhanced the epoxide selectivity.

1. Introduction

Zeolites have been widely used as solid catalysts in many processes of refining and petrochemical industry. The MCM-22 zeolite (IZA code MWW) is first identified by Leonowicz et al.[1] in 1994 to have the crystalline structure formed by vertically 30 aligning lamellar zeolite intermediate, and the material was patented in 1990 by Rubin and Chu in Mobil.[2] Since then, the two-dimensional (2D) layered zeolites have attracted great attention of the zeolite researchers. Owing to the importance of MCM-22 in practical applications to industrial chemical 35 processes, intensive studies have been devoted to preparing the

derivatives of layered zeolite materials, meeting the demands that the individual layer surfaces can be exposed, the resulting layers keep the original structure of the precursor, and most of the zeolite acidity remains in the final material. The important 40 achievements have been well summarized in a number of reviews and papers published in recent years.[3-4]

The as-made MCM-22 is the stacking of zeolitic sheets with repeating unit $d_{(001)}$ of 2.5 nm[5]. The two adjacent zeolitic sheets expand approximate 0.2 nm apart in the *c*-direction with the 45 openings of the cup-shaped structures facing each other. Upon calcination, 3D MWW zeolitic structure is formed by condensation of the Si-OH groups on contiguous sheets, generating 12-ring MWW cages (0.71 x 0.71 x 1.82 nm).

The MCM-22 zeolite was actually prepared earlier in 1984 by 50 Puppe and Weisser[6] as PSH-3 and in 1987 by Zones[7] as SSZ-25. Both aluminosilicates exhibited similar characteristic X-ray powder diffraction (XRD) patterns as MCM-22. In 1988, Bellussi et al.[8] reported the synthesis of a borosilicate zeolite (ERB-1), which is actually isostructural with the MCM-22 aluminosilicate.[9] 55 ERB-1 was the abbreviation of EniRicerche-Boralite-1 and was claimed by Bellussi et al. in their European patent.[8] Tatsumi et al.[10] and Wu et al.[11] successfully synthesized the titanosilicate zeolites, naming Ti-MWW and Ti-YNU-1, respectively, using

[1]*Department of Chemistry, National Taiwan University, Taipei 10617, Taiwan; Email:chem1301@ntu.edu.tw*
[2]*Key Laboratory for Green Chemical Process of Ministry of Education, School of Chemical and Pharmaceutical Engineering, Wuhan Institute of Technology, Wuhan 430074, China*
[3]*Research Division, National Synchrotron Radiation Research Center, Hsinchu 300, Taiwan.*

ERB-1 as the precursor.

The Ti-substituted zeolites, including ZSM-5, beta and mordenite, and Ti-MWW and Ti-YNU-1, have been reported to be efficient catalysts for the selective oxidation of a large family of organic substrates.[10, 11, 12-16,] However, the micropore structures restrict their uses in reactions involving molecules of relatively large diameters. Recently, Ryoo's group designed a series of gemini-type, polyquaternary ammonium surfactants that could generate micropores and mesopores simultaneously, and they applied the surfactant to synthesize ordered mesoporous structures (hexagonal or 3D) with thin zeolitic walls based on the dual-templating concept.[17] The drawbacks are the tedious procedure and cost of the specially designed surfactants.

To overcome the disadvantage of micropore sizes of MCM-22, the lamellar precursor has been converted into a micro- and mesoporous hybrid, MCM-36,[18] by swelling with organic surfactant followed by pillaring with polymeric silica. It can also be delaminated into ITQ-2,[19] which consists of aggregation of thin zeolite sheets of ca. 2.5 nm height through exfoliating the swollen precursor with ultrasound. Both MCM-36 and ITQ-2 have extremely high surface areas and the active sites are highly accessible by the bulky molecules.[5] Recently, analogous pillaring technique has also been applied to layered TS-1 materials prepared using Ryoo's recipe, and the resulting materials were found efficient catalysts for epoxidation of bulky organic molecules.[20] However, the incorporation of Ti in mesoporous materials or with open pore zeolites is still a challenge. The Ti-MWW and Ti-YNU-1 structures were not as stable as the siliceous MCM-22, which was the precursor to synthesize Ti-MCM-36. The procedure to prepare titanosilicates MCM-36 with mesopores by pillaring the Ti-WWW precursor with SiO_2 was very complicated because of the secondary hydrothermal process.[20,21] On the other hand, Corma et al.[22] prepared Ti-ITQ-2 by grafting titanocene onto the surface of siliceous ITQ-2 to ensure good accessibility of Ti sites. However, the Ti precursor is expensive.

Recently, a new approach for preparing Ti incorporated MCM-36 (named Si/Ti-MCM-36) was developed in our group by pillaring the MCM-22 precursor with titanosilicate clusters.[23] Nevertheless, the Si/Ti-MCM-36 material was found inactive in epoxidation reaction using peroxide as the oxidizing agent because the acidity generated by framework aluminium would catalyze the decomposition of peroxide during the reaction. Acid treatment to leach out framework aluminium was essential to activate Si/Ti-MCM-36. That prompts us to expand our investigation with ERB-1 precursor in preparation of Si/Ti-MCM-36. The Si/Ti ratios in the resulted Si/Ti-MCM-36(E) were controlled by varying the amounts of tetraethylorthosilicate (TEOS) and tetra-n-butylorthotitanate (TBOT) moieties. Indeed, the resultant Si/Ti-MCM-36(E) exhibited good catalytic performance in epoxidation of cyclohexene with tert-butyl hydroperoxide (TBHP).

2. Experimental Methods

2.1. Preparation of materials

The ERB-1 precursor (shortly termed ERB-1(P)) was prepared following the synthesis method reported by Millini et al.[9] with the molar ratio of Si: B: piperidine (PI): H_2O = 1: 0.75: 1.4: 19. ERB-1(P) was swollen by cetyltrimethylammonium bromide (CTMABr) in the presence of tetrapropylammonium hydroxide (TPAOH) using a solution with a relative weight ratio of TPAOH: CTMABr: H_2O = 1: 4: 330. The mixture was sealed in a flask and heated at 373 K for 16 h. The resulted material was isolated by filtration, washing with distilled water, and drying under vacuum. The swollen ERB-1 was dispersed in a mixture of TEOS and TBOT with the TEOS/TBOT molar ratio varied in 0:1, 5:1, 20:1, 40:1, 80:1, 120:1, up to ∞. The liquid/solid weight ratio was 1/10. After the mixture was stirred at 353K for 25 h, the solid was filtered and dried at ambient condition. The hydrolysis of TBOT and TEOS was carried out by suspending the dried solid in an aqueous solution at 313 K for 6 h at pH = 9 adjusted by 1 M NH_3. Finally, the sample was calcined at 723 K for 3 h in nitrogen and at 812 K for 6 h in air (heating rate of 2 K/min). The resultant materials were designated as xSi/Ti-MCM-36(E), where x is the Ti/Si molar ratio in the pillaring gel. The symbol (E) represents it is a derivative of ERB-1.

The acid treatment of 40Si/Ti-MCM-36(E) was carried out by refluxing the calcined sample in a 2 M HNO_3 solution at 353 K for 6 h and subsequent calcination at 833 K. The acid-treated sample is denoted as A-Si/Ti-MCM-36(E).

For comparison, the MCM-22 precursor (MCM-22(P)) was also synthesized. The procedure for preparing the corresponding Ti incorporated MCM-36 (xSi/Ti-MCM-36(M)) is the same as that stated above. Other titanosilicate Ti-YNU-1 and Ti-MWW were also prepared by hydrothermal synthesis method described in the literature.[24,25] TS-1 was synthesized using TEOS, TBOT and TPAOH.[26] After calcination at 823 K for 15 h, TS-1 was further washed with 2 M HNO_3 solution to remove any extra-framework Ti species.

2.2. Characterization

XRD patterns were recorded using a PANalytical X'Pert PRO diffractometer with a Cu-$K\alpha$ radiation (λ=1.5418 Å) operated at 40 mA and 45 kV. N_2 sorption isotherms were measured at 77 K on a Micrometerics TriStar 3000 analyzer after vacuum pretreating the samples at 473 K for 8 h. Total specific surface areas (S_{BET}) were calculated using the Brunauer-Emmett-Teller (BET) method, and the total pore volume (V_{total}) was evaluated from N_2 uptake at a relative N_2 pressure of 0.99. The t-plot was employed to evaluate the volume of micropores (V_{micro}). The corresponding pore size distribution (PSD) was determined using the desorption branches of the isotherms by Barrett-Joyner-Halenda (BJH) method. The argon sorption isotherms were recorded at 87 K with an automated volumetric analyser ASAP 2020 (Micromeritics Instrument Corp., USA), following the dynamic measurement mode.[27] The pore size distributions of micropores were based on the Horvath-Kawazoe plot. Diffuse reflectance (DR) UV-Vis spectra were recorded using a Hitachi U-3310 spectrometer equipped with an integrating sphere detector, and $BaSO_4$ was the reference. The elemental analyses were determined using Electron Probe Micro Analysis (EPMA) in JEOL JXA-8200 Electron Probe. Ti K-edge X-ray absorption spectra (XAS) were collected using the fluorescence mode at Beamlines 16A and 17C of the National Synchrotron Radiation

Research Center (NSRRC) at Hsinchu, Taiwan. Standard operating condition was 1.5 GeV and 350 mA. The photon energy was guided using a fixed-exit double-crystal Si(111) monochromator and calibrated with a metallic Ti foil (*K*-edge, 4966 eV). Scanning electron microscopy (SEM) photographs were taken using a JEOL JSM-7600F and Hitachi S-4800 Field Emission Scanning Electron Microscope. Transmission electron microscopy (TEM) photographs were obtained from a JEOL JEM-1200EX II Transmission Electron Microscope. High-resolution (HR) TEM photographs were taken with a Philips/FEI Tecnai 20 G2 S-Twin Transmission Electron Microscope. NH_3-TPD was conducted in a Micromeritics Autochem II chemisorption analyzer with a quartz reactor and 100 mg sample with particle size of 0.18-0.28 mm. The sample was preheated at 823 K for 1 h in a 30 mL/min (STP) flow of He. After cooling to 373 K, NH_3 was flowed through the sample for 1 h. The excess NH_3 was removed by purging with 30 mL/min He at 373 K for 2 h. Desorption was then performed under the same He flow with a ramp rate of 10 K/min up to 823 K.

2.3. Catalytic reaction

The catalytic activities of Si/Ti-MCM-36 materials were examined by carrying out liquid phase epoxidation of cyclohexene with TBHP (5.5 M in decane) at 353 K. Calcined samples were pre-dried at 423 K overnight before used as the catalysts. In a typical run, 50 mg of the catalyst in powder form was added in a mixture of 10 mmol cyclohexene, 3 mL decane, and 7 mmol TBHP heated in a two necked round-bottom flask with a stir bar and a water cooling condenser at 353 K to start the reaction. At specific reaction periods, the reaction mixtures were collected. After removal of solid catalysts, the liquid products were qualitatively analyzed by an Agilent HP 6890 gas chromatograph (GC) equipped with a mass spectrometry. The quantitative analysis was conducted with a Shimadzu GC-2014 instrument equipped with a FID detector, where cyclopentanone was used as an internal standard. The cyclohexene conversion and product selectivities were calculated by the following equations.

Conversion (%) = (formed derivatives of cyclohexene in mol / initial cyclohexene in mol) × 100.

Selectivity (%) = (specific product in mol / formed derivatives of cyclohexene in mol) ×100.
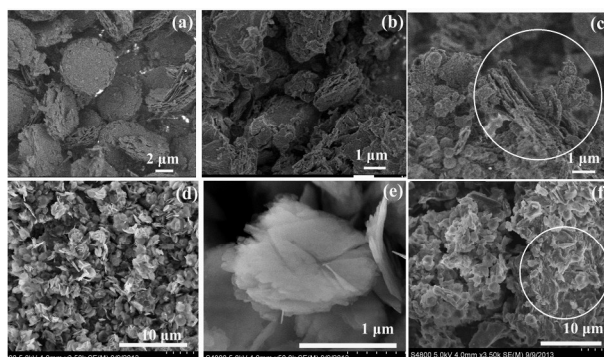
3. Results and Discussion

3.1. Comparison of Si/Ti-MCM-36 materials prepared from ERB-1 and MCM-22 precursors

The swelling treatment of MCM-22(P) with the mixture of TPAOH and CTMABr at elevated temperature resulted in partial dissolution of the framework silicon under such a high pH condition. This phenomenon is demonstrated in Table 1 that Si/Al ratio of MCM-22(P) markedly decreases from 15 to 10 after swelling treatment, consistent with that reported in the literature.[28] On the other hand, boron in ERB-1 was completely removed after swelling process. The elemental analysis results in Table 1 show that all the pillared MCM-36(E) samples do not contain boron anymore. These results imply that pure siliceous

MWW framework was obtained after swelling treatment of ERB-1. As to the Ti contents in the pillared samples, the Si/Ti ratio is 15.3 for 40Si/Ti-MCM-36(E) and 16 for 40Si/Ti-MCM-36(M). The values are close with each other, inferring that the intercalation of titanosilicate pillars in between the MWW layers is not affected by basal layer composition.

The scanning electron images of ERB-1, MCM-22, and the corresponding pillared products 40Si/Ti-MCM-36(E) and 40Si/Ti-MCM-36(M) are depicted in Fig. 1. The ERB-1 and MCM-22 precursors are all platelet morphologies, but the platelets of ERB-1 are larger than those of MCM-22 (about 2.5 μm vs. 1.5 μm in diameter and 1μm vs. 0.1 μm in thickness). Moreover, ERB-1 is dense piles of flaky crystals, while MCM-22 is irregular aggregates of inter-grown flakes. The pillared samples all show corrosive surfaces and edges, as well as cracks on the platelets. It is deduced that the dissolution of framework silica during the swelling treatment erodes the structure. For 40Si/Ti-MCM-36(E), it is clearly seen a large amount of petal-like particles smaller than 0.5 μm, which are likely the drop out from the platelets. In contrast, 40Si/Ti-MCM-36(M) is obvious the large aggregate particles with compact stacking of layers.
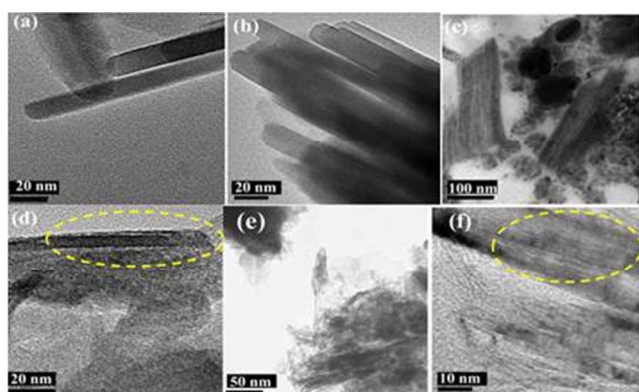

Figure 1. The scanning electron micrographs of (a) calcined EBR-1, (b) and (c) 40Si/Ti-MCM-36(E) from JEOL JSM-7600F, (d) and (e) calcined MCM-22; (f) 40Si/Ti-MCM-36(M) from Hitachi S-4800 Field Emission Scanning Electron Microscope.
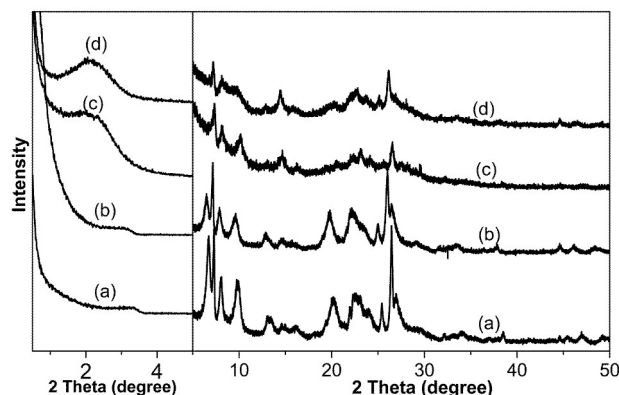
High resolution lattice images obtained by transmission electron microscopy confirm the generation of MCM-36 as shown in Fig. 2. The ERB-1 and MCM-22 precursors consist of thin circular disks and sharp facets. The thickness of ERB-1 and MCM-22 disks is about 15-20 nm, similar to the literature report.[28] The pillared samples show stacked layers and some disordered domains. For 40Si/Ti-MCM-36(M), the intercalated structure and some of the exfoliated layers can be identified. The repeated distance between the pillared layers is about 2 nm. As to 40Si/Ti-MCM-36(E) prepared by pillaring ERB-1(P), more ordered expanded layers with 2 nm in distance can be found than that prepared from MCM-22(P). However, some dense packed layers can also be seen (Fig. 2c).

The small- and wide-angle XRD patterns of the samples are shown in Fig. 3(A) and (B), respectively. Both the ERB-1 and MCM-22 precursors show (001) diffraction at about 3°, corresponding to the unit cell of 2.7 nm for MWW layers aligning along the *c*-direction. The pillared MCM-36 samples show shifts of the (001) reflection down to around 2°, corresponding to *d*-spacing of 5.0 nm. Meanwhile, the (002) diffraction at 6.5° of the precursors almost disappears. All these phenomena indicate the

successful expansion of MWW layers. The position of intra-layer (hk0) diffraction in pillared samples, such as the (100), (220), and (310) peaks at about 7.1°, 25.1° and 26.1°, remain conspicuously unchanged, which indicates that the internal structure of MWW
5 layer is retained. On the other hand, the merging of (101) and (102) diffraction peaks of MCM-22(P) at roughly 8° and 10° as a broad band for MCM-36(M) demonstrates the loss of stacking order of the layers.[29] In contrast, MCM-36(E) still retains discrete (101) and (102) peaks of the precursor, inferring that a small
10 portion of ERB-1(P) may not be effectively expanded and pillared in the process. This result is consistent with the observation in TEM experiments, where some dense packed layers can be seen in MCM-36(E). It is probably due to that ERB-1(P) contains larger platelet particles, and the diffusion and
15 homogeneous spreading of the pillaring reagents into inner domain of the platelets is difficult.

Figure 2. Transmission electron micrographs of (a) ERB-1(P), (b)
20 MCM-22(P); (c), (d) 40Si/Ti-MCM-36(E), and (e), (f) 40Si/Ti-MCM-36(M). ((a), (b), (d), (f) from Philips/FEI Tecnai 20 G2 S–Twin, and (c), (e) form JEM-1200EX II Transmission Electron Microscope).
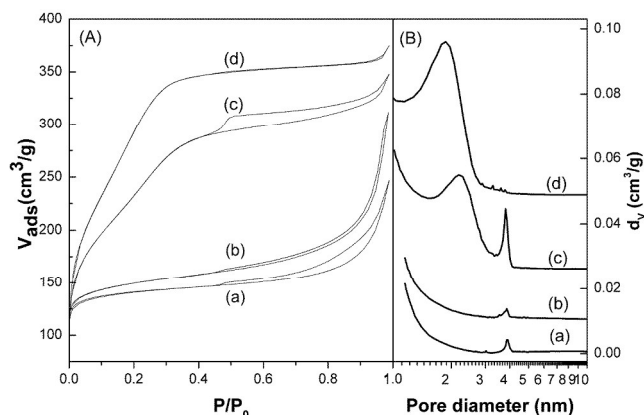

25 **Figure 3.** XRD patterns of (a) ERB-1(P), (b) MCM-22(P), (c) 40Si/Ti-MCM-36(E) and (d) 40Si/Ti-MCM-36(M).

The N_2 sorption data are shown in Fig. 4. The sorption isotherms of both ERB-1 and MCM-22 zeolites are Type I
30 isotherm (Fig. 4(A)), characteristics of microporosity. On the other hand, both pillared MCM-36 samples show Type IV isotherms with an increase in the adsorption volume at relative pressure of 0.2~0.4, indicating the presence of mesopores. The

pore diameter determined by BJH method is about 2 nm (Fig.
35 4(B)). The larger intensity of the 2 nm peak on Si/Ti-MCM-36(E) than Si/Ti-MCM-36(M) quantitatively verifies that ERB-1(P) is more efficient than MCM-22(P) in generating 2 nm mesopores by pillaring. Moreover, a hysteresis loop is seen on 40Si/Ti-MCM-36(M) sample at P/P_0 greater than 0.4, indicating the presence of
40 slit-shaped mesopores of larger sizes. The increases in adsorption volume at high partial pressure are also observed on MCM-22 and ERB-1 zeolites, and that is responsible for the sharp peaks at about 4 nm in the BJH pore size distribution (PSD) profiles in Fig. 4(B). These mesopores are likely due to the non-rigid
45 aggregates of plate-like particles or crystal defects, and they are not present on MCM-36(E).

The intercalation efficiency is judged by the textural properties derived from N_2 sorption data as shown in Table 1. The more effectively pillared sample is considered to contain larger S_{BET}
50 and V_{meso}. ERB-1 zeolite has slightly lower S_{BET} and V_{total} than MCM-22, probably because of the larger particle size. However, the pillared Si/Ti-MCM-36(E) samples have much higher S_{BET} and V_{meso} than Si/Ti-MCM-36(M). Therefore, the pillaring efficiency of ERB-1 is much better than MCM-22. The high
55 pillaring efficiency of ERB-1 is probably due to the presence of lattice defects generated during the layer expansion process, where almost all boron are leached out from the framework. These defects facilitate the diffusion of pillaring reagents into the interlayer void space for pillaring.
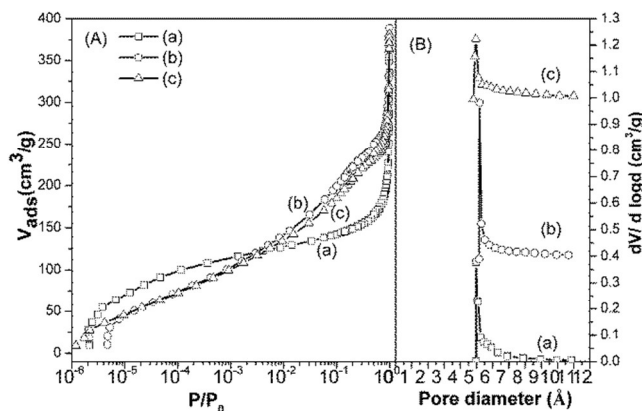

60
Figure 4. (A) N_2 adsorption/desorption isotherms and (B) BJH pore size distribution of (a) ERB-1, (b) MCM-22, (c) 40Si/Ti-MCM-36(M), and (d) 40Si/Ti-MCM-36(E).

The increases in the V_{meso} and reduction in the V_{micro} values of
65 Si/Ti-MCM-36 materials in comparison to those of MCM-22 and ERB-1 are due to that the portion of the micropores formed in condensation of adjacent MWW layers was replaced by the interlayer mesopores formed by pillaring in MCM-36. This phenomenon is more clearly shown in the argon isotherms of
70 ERB-1 and Si/Ti-MCM-36(E) in Fig. 5(A). The Ar uptake in the low relative pressure ($<10^{-2}$) corresponding to micropore condensation is larger on ERB-1, while the uptake in the relative pressures of 0.2−0.4 corresponding to mesopore condensation is significantly increased on Si/Ti-MCM-36(E). Similar observation
75 was reported by Zukal and Kubu[27] on pillared products of IPC-3(P) and MCM-22(P). Moreover, the preservation of a portion of the micropores in the MCM-36 was confirmed by the reserved Ar

uptake in the low relative pressure (Fig. 5(A)), which corresponds to the sharp PSD peaks at about 0.5 nm in Fig. 5(B). In the high relative pressure region (0.01-1), the argon isotherms of ERB-1 and Si/Ti-MCM-36(E) in Fig. 5(A) are similar as those of nitrogen in Fig. 4(A). Therefore, the derived S_{BET}, V_{total}, V_{micro} and V_{meso} from Ar sorption isotherms are also very similar to those from N$_2$ isotherms.

In order to examine the possibility that new amorphous materials are generated during the pillaring process, the filtrate of the TEOS and TBOT pillaring reagents for 40Si/Ti-MCM-36(E) was precipitated by the same hydrolysis and drying procedures as those for preparing Si/Ti-MCM-36(E). The resultant precipitate was confirmed to be actually TiO$_2$-SiO$_2$ glass with titania-rich cores covered by silica-rich patches,[23] similar to those synthesized by Hutter et al.[30] and Miller et al.[31], and the material exhibits almost no N$_2$ uptake in the N$_2$ sorption characterization. Therefore, the contribution of surface area from new amorphous materials is negligible.

The elemental analysis data by EPMA shown in Table 1 demonstrate that 40Si/Ti-MCM-36(E) has higher Ti content than 40Si/Ti-MCM-36(M) (Si/Ti molar ratio of 15.3 vs. 50), even though both materials were prepared with the same amounts of TEOS/ TBOT mixture. The DR UV-Vis spectra of the MCM-36 samples pillared with TEOS/TBOT mixtures of molar ratios 40 are shown in Fig. 6(A). These two pillared samples have two peaks at 220 and 260 nm. The 220 nm band, assigned to charge transfer from O^{2-} to Ti^{4+} of the tetrahedral (T$_d$) coordination, while the 260 nm band is attributed to charge transfer from O^{2-} to Ti^{4+} in octahedral (O$_h$) coordination. The latter is considered due to extra-framework TiO$_2$ species.[32] Because 40Si/Ti-MCM-36(E) has stronger intensity of 260 nm peak than 40Si/Ti-MCM-36(M), more TiO$_2$ clusters are formed on 40Si/Ti-MCM-36(E). It is attributed to that the Ti content in 40Si/Ti-MCM-36(E) is more than three times higher than that of 40Si/Ti-MCM-36(M).
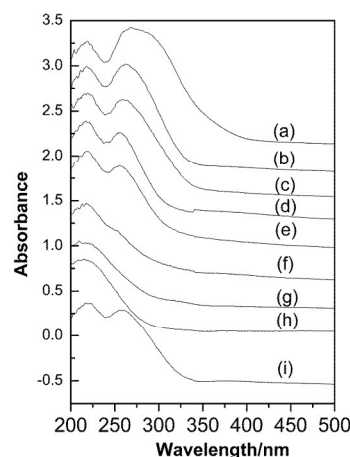

Figure. 5. (A) log plots of Ar sorption isotherms and (B) Horvath-Kawazoe differential pore volume plots of (a) ERB-1, (b) 40Si/Ti-MCM-36(E) and (c) A-Si/Ti-MCM-36(E).
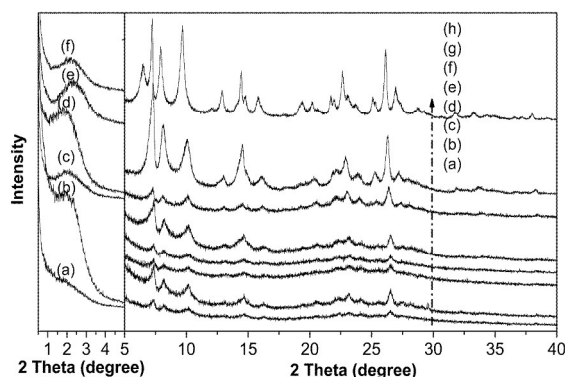
3.2. Influence of Si/Ti ratio of pillaring sol on the MCM-36

The elemental analysis results in Table 1 show that the amount of Ti incorporated in Si/Ti-MCM-36(E) increases with the decrease of TEOS/TBOT ratio in the pillaring mixture. In other words, the Si/Ti ratio in the resulted Si/Ti-MCM-36(E) is proportional to that of pillaring moieties.

XRD patterns of the pillared ERB-1 samples with different TEOS/TBOT ratios in the pillaring mixture are compared with that of calcined EBR-1 (Fig. 7). The appearance of obvious (001) diffraction peak at 2° on all Si/Ti-MCM-36(E) samples confirm the effective pillaring with the TEOS/TBOT mixture. The only exception is samples 0Si/Ti-MCM-36(E) which is pillared with pure TBOT. The retention of discrete (101) and (102) diffraction peaks for the pillared ERB-1 indicate that a small portion of ERB-1(P) is not effectively expanded and pillared in the process. Again, it should be attributed to the large particle sizes of ERB-1(P).

Figure 6. DR UV-Vis spectra of (a) 0Si/Ti-MCM-36(E), (b) 40Si/Ti-MCM-36(E), (c) 80Si/Ti-MCM-36(E), (d) 120Si/Ti-MCM-36(E), (e) 140Si/Ti-MCM-36(E), (f) A-Si/Ti-MCM-36(E), (g) Ti-MWW, (h) Ti-YNU-1 and (i) 40Si/Ti-MCM-36(M).

Figure 7. Small angle and wide angle XRD patterns of (a) 0Si/Ti-MCM-36(E), (b) 40Si/Ti-MCM-36(E), (c) 80Si/Ti-MCM-36(E), (d) 120Si/Ti-MCM-36(E), (e) 140Si/Ti-MCM-36(E), (f) A-Si/Ti-MCM-36(E), (g) Ti-MWW and (h) Ti-YNU-1.

The N$_2$ sorption isotherms and BJH PSD profiles are shown in Fig. 8, and the derived textual properties are shown in Table 1. The intercalation efficiency is judged by the amount of N$_2$ uptakes at relative pressures of 0.2 to 0.4, which corresponds to the peaks around 2 nm in the BJH PSD profiles. Again, 0Si/Ti-MCM-36(E) has very low N$_2$ uptake at this relative pressure region and weak intensity of the 2 nm peak. The low intercalation

efficiency with pure TBOT is deduced by that the high viscosity of pure TBOT restricts its diffusion into the interlayer of swollen MWW layers. However, the viscosity is lowered down by mixing TBOT with TEOS, and it becomes easier to permeate into the interlayer of swollen MWW layers and form titanosilicate pillars after hydrolysis.

Table 1. The physico-chemical properties of the MCM-36 samples with different Si/Ti ratio.

Sample	Si/Ti[a]	Si/M(III)[a]	S_{BET} (m²/g)	V_{total}	V_{micro}[b] (cm³/g)	V_{meso}[c]
ERB-1	N.A.	57	449	0.31	0.18	0.13
Swollen MCM-22	-	∞	-	-	-	-
0Si/Ti-MCM-36 (E)	11	∞	641	0.35	0.09	0.26
40Si/Ti-MCM-36 (E)	15.3	∞	1118	0.56	0.01	0.55
80Si/Ti-MCM-36 (E)	29.6	∞	893	0.54	0	0.54
120Si/Ti-MCM-36 (E)	34	∞	947	0.58	0.02	0.56
140Si/Ti-MCM-36(E)	75.3	∞	1002	0.65	0	0.65
A-Si/Ti-MCM-36(E)	173	∞	900	0.54	0.02	0.52
MCM-22	-	15	479	0.36	0.18	0.19
Swollen MCM-22	-	10				
40Si/Ti-MCM-36(M)	50	16	843	0.50	0.03	0.47
Ti-YNU-1	130	N.A.	554	0.50	0.20	0.30
Ti-MWW	102	N.A.	434	0.33	0.17	0.17
TS-1	154	N.A.	390	0.18	0.10	0.08

(a) elemental composition of Si/Al(III) or Si/B(III) from EPMA; (b) the volume of micropores from *t*-plot(cm²/g);
(c)V_{Meso} is calculated by V_{total} - V_{micro} (cm²/g).

The prepared samples were analyzed by DR UV-Vis spectroscopy in order to gain information about the coordination environment of the Ti centers. Fig. 6 shows that all the DR UV-Vis spectra of Si/Ti-MCM-36 samples, except 0Si/Ti-MCM-36(E), lack for absorption above 330 nm, indicating no formation of TiO_2. All the pillared samples have two peaks at 220 and 260 nm. Moreover, the intensity of the ~260 nm peak obviously decreased with the decrease of Ti loadings. Therefore, to reduce Ti centers of O_h coordination, which corresponds to TiO_2 clusters, the Si/Ti ratio in the pillaring agent should be relatively high.
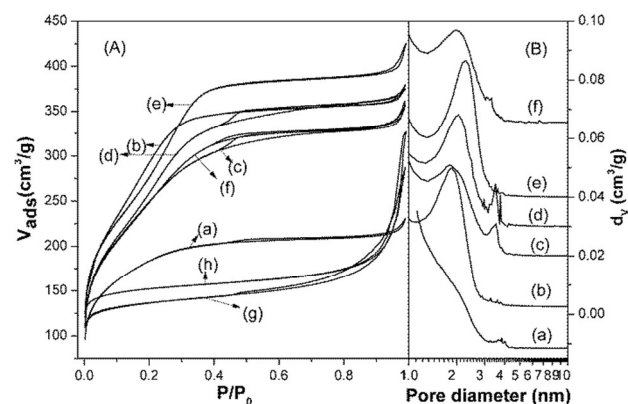
3.3. Local environment of pillared Ti

The coordination environment of Ti was further studied by taking XAS spectra at the Ti *K* edge. The X-ray absorption near edge structure (XANES) can probe the symmetry of Ti coordination in a qualitative manner by comparison of the pre-edge peaks with those of reference materials, including

crystalline TiO_2 and Ti-YNU-1. Ti-YNU-1 has been reported by Ruan et al.[24] and also confirmed by our results of UV-Vis spectra to contain exclusively 4-coordinated Ti which is incorporated in the framework of MWW zeolite (Fig. 6). In the case of Ti in O_h coordination structures, rutile and anatase are typical examples. Fig. 9 shows that the pre-edge features of rutile and anatase give rise to three peaks denoted A_1, A_2 and A_3. The intensity of the A_2 peak increases with increasing the site distortion.[33]

The A_2 peak of sample 0Si/Ti-MCM-36(E) which is pillared by pure TBOT is close in energy position to those of rutile and anatase, and the intensity is lower than those of other Si/Ti-MCM-36 and Ti-YNU-1 samples. In addition, the shoulder peaks of A_1 and A_3 can also be seen. This result is consistent with the UV-Vis results that the sample pillared with pure TBOT has TiO_2 clusters as the pillars. In contrast, the A_1 and A_3 peaks merge with the A_2 peak in the Si/Ti-MCM-36(E) samples pillared with TEOS/TBOT mixtures.

Farges et al.[34] conducted an extensive study to distinguish between fourfold, fivefold, and sixfold coordination symmetry around the Ti atom by determination of both the distinctive pre-edge peak energy and the normalized intensity of A_2 pre-edge peak using titanium-containing reference compounds. The intensity of normalized A_2 pre-edge peaks in the pillared ERB-1 samples prepared with TEOS/TBOT mixtures is not as intense as that of Ti-YNU-1. Moreover, the energy position of the A_2 peaks shifts to higher energy comparing with that of Ti-YNU-1. Based on the results measured by Farges et al.[34], the pre-edge features observed on the pillared ERB-1 samples suggest that the Ti is present in both 4- and 6-coordinated environments in Si/Ti-MCM-36(E) but the amount of 6-coordinated Ti is almost diminished when larger TEOS/TBOT ratio is used for pillaring. That is consistent with the results of UV-Vis spectra.

Figure 8. (A) N_2 adsorption/desorption isotherms (B) BJH pore size distribution of (a) 0Si/Ti-MCM-36(E), (b) 40Si/Ti-MCM-36(E), (c) 80Si/Ti-MCM-36(E), (d) 120Si/Ti-MCM-36(E), (e) 140Si/Ti-MCM-36(E), (f) A-Si/Ti-MCM-36(E), (g) Ti-MWW and (h) Ti-YNU-1.

In addition to the pre-edge features, the post-edge features (as depict in Fig. 9) can also provide information concerning the local structure of Ti. Both anatase and rutile exhibit white line features at about 4987 eV. Rutile exhibits several additional maxima at 4992, 5004, 5020, and 5048 eV, while anatase exhibits three resolvable maxima in the range of 4995−5003 eV, in

consistence with previous work.[32] It can be seen that the post-edge features in the pillared MCM-36 samples are less distinct than in the reference oxides. The lack of distinct features in post-edge range is due to the loss of long- and medium-range ordered structures, indicating that Ti is not present as crystalline TiO_2 particles.
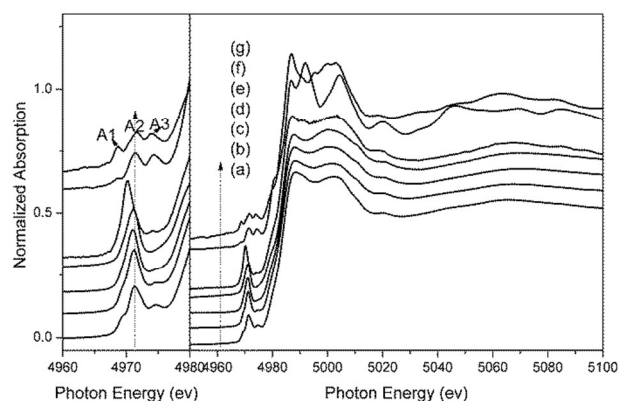
The extended X-ray absorption fine structure (EXAFS) spectra of the pillared samples are compared with those of the reference samples in Fig. 10. Although rutile and anatase have slightly different oscillations in their Fourier transform Ti K-edge spectra, the first intense peak at 1.5 Å (not phase corrected) is corresponding to the nearest O atoms around Ti, which should be 1.95 Å according to crystallographic data. The second peak appearing at about 2.2 Å for rutile or 2.5 Å for anatase is assigned to neighbouring Ti, while the pronounced third peak at about 3 Å (not phase corrected) are attributable to the second shell O atoms.[32] In the case of Ti-YNU-1, the nearest O atoms scattering feature shows a slight shorter Ti-O distance, comparing with those of reference oxides. The shorter Ti-O distance strongly suggests the presence of a fourfold coordination of Ti. On the other hand, most of the titanosilicate pillared samples and Ti-YNU-1 show only very weak or no oscillation peaks at larger distances other than the first intense peak. However, 0Si/Ti-MCM-36(E) which is pillared with pure TBOT has the second peak at 2.3 Å (not phase corrected) corresponding to the Ti-O-Ti linkages. It is also noticed that the intensity of this second peak at 2.3 Å increases in other titanosilicate pillared samples as Si/Ti ratio decreases. These results confirm that pure TBOT forms TiO_2 clusters as the pillars and Ti is not dispersed in the silica matrices, while most of the Ti in titanosilicate pillared samples are well distributed in the silica matrices forming Ti-O-Si linkage rather than Ti-O-Ti linkage.

The Ti K–edge XANES and the UV-Vis spectra of the 140Si/Ti-MCM-36 samples demonstrate that Ti(IV) is well dispersed by pillaring the MWW layers with Ti/Si mixed oxide. In contrast, the Ti grafting MCM-36 samples prepared by grafting titanium tetra-isopropoxide on Si-MCM-36 have pronounced absorption above 300 nm in the UV-Vis spectra, inferring the formation of TiO_2 clusters or crystallites on these samples.[23] Therefore, the 2 nm mesopores in Si/Ti-MCM-36(E) samples can be confirmed to be due to the interlayer expansion of MWW layers by titanosilicate pillars. However, the 4-coordinated Ti(IV) is considered to disperse not only in the pillars but also in the MWW framework. The defect sites left behind by the B removal during the post treatment process can be reinserted by Ti and Si. Both the Ti sites situating in the MWW framework and in the pillars should be accessible by the reactants.
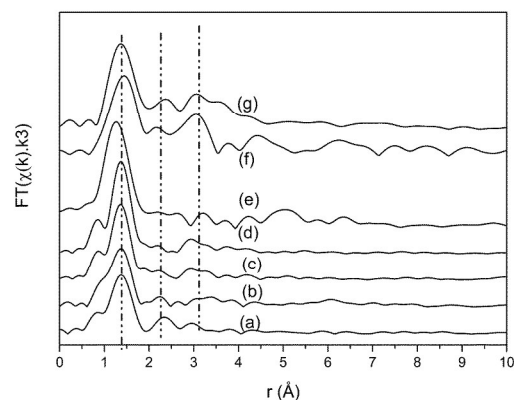
3.4. The influence of acid treatment on the Si/Ti-MCM-36

The post modification of 40Si/Ti-MCM-36 with 2 M HNO_3 was performed at 353 K for 6 h. As shown in Table 1, the acid treatment causes a dramatic increase of Si/Ti ratios in the samples, indicating that Ti is leaching from the structure. The XRD patterns of 40Si/Ti-MCM-36(E) before and after acid treatment are given in Fig. 7(f). The retention of the broad X-ray diffraction in the small angle region confirms the conservation of pillaring structure. The split peaks of (101) and (102) at $2\theta = 8$ and 10° attributed to the ordered stacking of the MWW layers along the c-direction are still seen. Moreover, the well-resolved

(100) and (310) peaks corresponding to diffractions from the ab plane are all retained. It can be concluded that the structures of MWW basal layer and the pillared MCM-36 structure are well preserved during acid treatment.

Figure 9. Ti K-edge XANES of (a) 0Si/Ti-MCM-36(E), (b) 40Si/Ti-MCM-36(E), (c) 140Si/Ti-MCM-36(E), (d) A-Si/Ti-MCM-36(E), (e) Ti-YNU-1, (f) rutile and (g) anatase TiO_2.

Figure 10. Fourier transform k3-weighted Ti EXAFS spectra in R-spacing of (a) 0Si/Ti-MCM-36(E), (b) 40Si/Ti-MCM-36(E), (c) 140Si/Ti-MCM-36(E), (d) A-Si/Ti-MCM-36(E), (e) Ti-YNU-1, (f) rutile and (g) anatase TiO_2.

The influence of acid treatment on the textural properties was examined by N_2 and Ar physi-sorption as illustrated in Fig. 8A(f) and Fig. 5A(c). The shape of sorption isotherm is almost the same as that of pristine 40Si/Ti-MCM-36. However, the acid treated samples show slightly lower amounts of N_2 or Ar uptakes at P/P_0 of 0.2−0.4. In Fig. 8B(f) of PSD profiles, the peak corresponding to 2 nm pores weakens and broadens. These results infer that the 2 nm mesopores generated by titanosilicate pillars are partially destructed by the acid treatment. Table 1 shows that the surface area decreases from 1118 to 900 m^2/g, while little change is seen in pore volumes. In the micropore region, the PSD profile of acid-treated 40Si/Ti-MCM-36 still has the peak corresponding to 0.5 nm (Fig. 5B(c)), suggesting the preservation of micropore systems of MWW structure after acid treatment.

The UV-Vis spectrum of the acid treated sample is shown in Fig. 6(f). It is noticed that the shoulder peak at 260 nm, attributed to O_h coordinated Ti species, vanishes obviously after acid treatment. The remained narrow 220 nm band is characteristics of T_d coordinated Ti. These results indicate that acid treatment removes Ti in O_h coordination and leaves T_d coordinated Ti in A-Si/Ti-MCM-36.

The Ti K-edge X-ray absorption spectra further confirm the coordination environment of Ti species in the acid-treated Si/Ti-MCM-36(E). Fig. 9(d) shows that A-Si/Ti-MCM-36 has only one A_2 pre-edge peak, which is similar to that of 140Si/Ti-MCM-36(E) and Ti-YNU-1. The Fourier transform k_3-weighted EXAFS spectrum in Fig. 10(d) also shows that the peak at 2.2~2.5 Å (not phase corrected) corresponding to Ti-O-Ti linkages of pristine 40Si/Ti-MCM-36(E) (Fig. 10(b)) is diminished. This result is consistent with the results of UV-Vis spectra that after acid treatment the TiO_2 species in the 40Ti/Si-MCM-36 is removed. The residual Ti species in A-Si/Ti-MCM-36(E) must be homogeneously dispersed in the silica framework forming the Ti-O-Si linkage, as that of Ti-YNU-1.

The acidities of the ERB-1 derivatives are studied by carrying out NH_3-TPD experiments and the results are shown in Fig. 11. The large decrease in acid amount from ERB-1 to 40Si/Ti-MCM-36(E) was attributed to the loss of boron, which is the source of acid sites, from the zeolite framework during swelling process. Further loss of acid sites is seen after acid treatment. That can be explained by leaching of the trace amount of boron remaining in Si/Ti-MCM-36(E), in which the boron content is below the detecting limit of EPMA technique. A-Si/Ti-MCM-36(E) is similar to Ti-YNU-1 in almost no adsorption of NH_3. Since Ti-YNU-1 has been identified to have boron completely removed from silica framework,[11] the results of NH_3-TPD experiments confirm that acid treated A-Si/Ti-MCM-36(E) material is also composed of titanosilicate only.
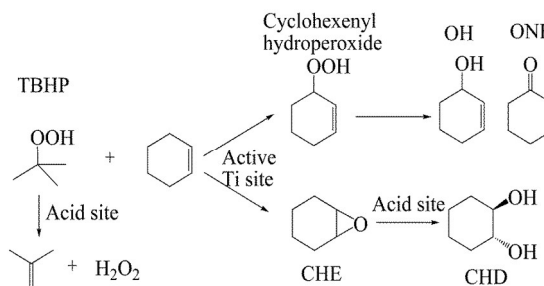
3.5. Catalytic properties of Si/Ti-MCM-36(E)

Titanium incorporated catalysts are among the most important oxidation catalysts for epoxidation of alkenes.[32] The success of incorporating Ti into MCM-36 started from ERB-1 encouraged us to investigate its catalytic behaviors in oxidation of bulky molecules. The epoxidation of cyclohexene using TBHP as the oxidant was the test reaction. Scheme 1 illustrates some of the typical products proposed in the previous studies.[32] The cyclohexene epoxide (CHE) is the target product, and 1,2-cyclohexanediol (CHD) is obtained by subsequent hydrolysis of CHE over acidic sites. Moreover, 2-cyclohexen-1-ol (OH) and 2-cyclohexen-1-one (ONE) can also be formed through allylic oxidation.[35]

Fig. 12 shows the results of cyclohexene epoxidation as a function of time-on-stream over xSi/Ti-MCM-36(E) and Ti-YNU-1. No products were detected without the catalysts. The epoxide yield and turnover number (TON) after 6 h reaction period are depicted in Fig. 13. As expected the cyclohexene conversion increases with time on stream and reaches the equilibrium after 10 h. However, the selectivities of CHE, CHD and OH are almost unchanged with time on stream.
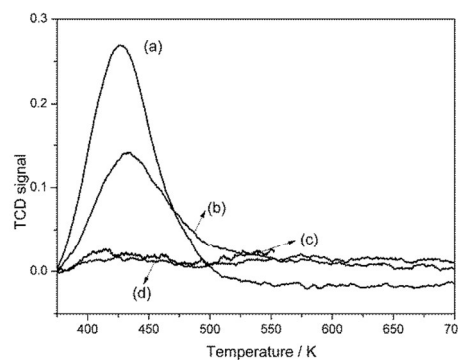
Acid treated A-Si/Ti-MCM-36(E) catalyst was found to have the highest cyclohexene conversion and CHE selectivity as well as relatively low selectivities of CHD and OH + ONE. The catalytic performance of A-Si/Ti-MCM-36(E) is similar to that of Ti-YNU-1. Both A-Si/Ti-MCM-36(E) and Ti-YNU-1 contain only T_d-coordinated Ti and has relatively low Ti contents among the studied catalysts. This is evidence that the isolated T_d-coordinated Ti is the active site for epoxidation reaction. The low CHD selectivities over A-Si/Ti-MCM-36(E) and Ti-YNU-1 indicate that the hydrolysis of CHE to form CHD is less favorable on these catalysts than the xSi/Ti-MCM-36(E) catalysts. Since A-Si/Ti-MCM-36(E) and Ti-YNU-1 catalysts lack of acid sites, their surfaces seem to be more hydrophobic and the hydrolysis of CHE to form CHD is suppressed.

As to the xSi/Ti-MCM-36(E) catalysts without acid treatment, higher cyclohexene conversions but lower CHE selectivities are obtained over xSi/Ti-MCM-36(E) with larger Ti contents or lower Si/Ti ratios (Figs. 12A and 12B). This kind of reverse trends with Ti content in xSi/Ti-MCM-36(E) catalysts are also observed on the TON of cyclohexene and CHE yield shown in Fig. 13. The increase of the Ti content in MCM-36 is synchronized with the increase in O_h-coordinated Ti species. These results demonstrate that both T_d and O_h-coordinated Ti species are active in cyclohexene oxidation. However, only the T_d-coordinated Ti is active for cyclohexene epoxide formation, while O_h-coordinated Ti species are more favourable for allylic oxidation to form cyclohexanol and cyclohexanone by-products.[32, 36]

Scheme 1. Reaction scheme of epoxidation of cyclohexene and possible by-products.
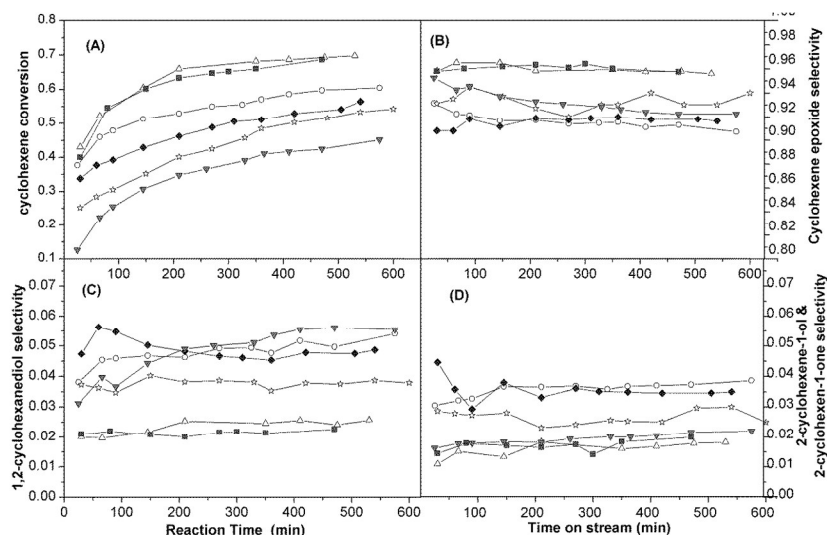

Figure 11. NH_3 TPD spectra of (a) ERB-1, (b) 40Si/Ti-MCM-36(E), (c) Ti-YNU-1 and (d) A-Si/Ti-MCM-36(E).

Journal Name

Dynamic Article Links ▶

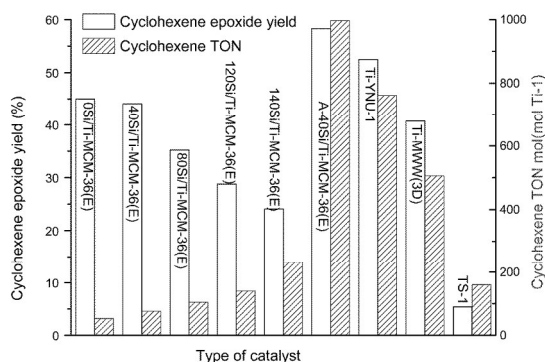## ARTICLE TYPE

Figure 12. (A) Cyclohexene conversion, (B) cyclohexene epoxide selectivity, (C) 1,2-cyclohexanediol selectivity and (D) 2-cyclohexene-1-ol selectivity vs TOS for (△) A-Si/Ti-MCM-36(E), (■) Ti-YNU-1, (○) 40Si/Ti-MCM-36(E), (◆) 80Si/Ti-MCM-36(E), (☆) 120Si/Ti-MCM-36(E) and (▼) 140Si/Ti-MCM-36(E).

Figure 13. Epoxide yield and turnover number for the epoxidation of cyclohexene over xSi/Ti-MCM-36(E), Ti-YNU-1, Ti-MWW and TS-1. Reaction conditions: 0.05 g of catalyst, 10 mmol of alkene, 5 mmol of TBHP (60 wt %), 3 mL of decane solvent, 353 K, 2 h.

Fig. 13 also compares the catalytic cyclohexene epoxidation over titanosilicates with different pore sizes and structures, including xSi/Ti-MCM-36(E), A-Si/Ti-MCM-36(E), Ti-YNU-1, Ti-MWW and TS-1. The turnover number (TON) was calculated based on the number of cyclohexene converted per Ti site in 2 h of reaction period. The cyclohexene TONs increase with the decrease of Ti contents in the xSi/Ti-MCM-36 catalysts. This phenomenon is also evidence that the T_d-coordinated Ti is the active site for epoxidation. TS-1 which contains pores of 5.5 Å shows the lowest activity, apparently due to the limitation of the pore diameter from diffusion of cyclohexene and TBHP inside the pore structure. Ti-MWW zeolite shows higher activity than

most of Si/Ti-MCM-36(E) owing to its large outer surfaces of the crystals. The Ti species located on the side pockets of Ti-MWW crystal surfaces are accessible by the bulky molecules. On the other hand, Ti-YNU-1 having the same basic building unit as Ti-MWW but with expanded interlayer windows from 10 to 12-ring and enlarged 2.59Å interlayer spacing has higher catalytic activity than Ti-MWW.[24,37] Nevertheless, A-Si/Ti-MCM-36(E) owned the expanded interlayer 2 nm mesopores is superior to the other catalysts in consideration of cyclohexene TON and epoxide yield. Therefore, the mesoporous A-Si/Ti-MCM-36(E) is a promising catalyst applicable to the oxidation reaction involving bulky substrates.

4. Conclusions

A titanosilicate pillared MCM-36 was prepared from the ERB-1 precursor, which is a borosilicate analogue of MCM-22 zeolite. The procedure included swelling with CTMABr and TPAOH, followed by pillaring the MWW sheets with titanosilicate formed via hydrolysis of interlayer TEOS and TBOT. Almost all the boron were expelled from the MWW frameworks during the swelling treatment of ERB-1. The N_2 sorption data showed that ERB-1 was more effectively pillared than MCM-22 in generation of 2 nm interlayer mesopores. Moreover, the ordered stacking of layer structure was better preserved in pillared ERB-1 than MCM-22 based on XRD results. It is attributed to that the small petal-like particles are generated in the swollen EBR-1, and they are more ready to intercalation than the large aggregated particles of swollen MCM-22.

The elemental analysis data by EPMA showed that 40Si/Ti-MCM-36(E) has higher Ti content than 40Si/Ti-MCM-36(M) even they were prepared with the same ratio of TEOS/TBOT

Journal of Materials Chemistry A Accepted Manuscript

moiety. The Si/Ti ratios in the Si/Ti-MCM-36(E) materials were proportional to that of TEOS/TBOT moiety used for pillaring. In addition, the ratio of T_d/O_h-coordinated Ti in Si/Ti-MCM-36(E) increases with the increase of TEOS/TBOT ratio.

The subsequent acid treatment on Si/Ti-MCM-36(E) could thoroughly eliminate the acidity of Si/Ti-MCM-36 without significant influence on the morphology and pillared structure. Meanwhile, most of the O_h-coordinated Ti species in A-Si/Ti-MCM-36 were removed, while T_d-coordinated Ti was retained as catalytic active sites for cyclohexene epoxidation toward CHE. Acid treatment also enhanced the surface hydrophobicity, which suppressed the hydrolysis of CHE to form CHD. In comparison to microporous Ti-containing zeolites, such as Ti-YNU-1, Ti-MWW and TS-1, the titanosilicate pillared MCM-36 prepared from ERB-1 showed the highest catalytic activity and was a promising epoxidaiton catalyst for processing the substrates with large molecular dimension.

Acknowledgments

References

1. Leonowicz M. E., Lawton J. A., Lawton S. L. and Rubin M. K., *Science*, 1994, **24**, 1910.
2. Rubin M. K. and Chu P., U.S.4954325, 1990.
3. Roth W. J. and Cejka J., *Catalysis Science & Technology*, 2011, **1**, 43.
4. Roth W. J., Nachtigall P., Morris R. E. and Čejka J., *Chem. Rev.*, 2014, **114**, 4807.
5. Díaz U., *Chem. Eng-new. York.*, 2012, **2012**, 1.
6. Puppe L. and Weisser J., U.S. 4439409, 1984.
7. Zones S. I., ed. C. RES, EP0231860, 1987.
8. Bellussi G., Perego G., Clerici M. G. and Giusti A., EP293032 1988.
9. Millini R., Perego G., Parker J. W. O., Bellussi G. and Carluccio L., *Micro. Mater.*, 1995, **4**, 221.
10. Wu P., Tatsumi T., Komatsu T. and Yashima T., *Chem. Lett.*, 2000, **29**, 774.
11. Fan W. B., Wu P., Namba S. and Tatsumi T., *Angew. Chem. Int. Ed.*, 2004 **43**, 236
12. Notari B., in *Adv. Catal.*, eds. D. D. Eley, Werner O. Haag and B. Gates, Academic Press, 1996, pp. 253.
13. Notari B., *Catal. Today*, 1993, **18**, 163.
14. Clerici M. G. and Ingallina P., *J. Catal.*, 1993, **140**, 71.
15. Tatsumi T., Nakamura M., Negishi S. and Tominaga H.-o., *Chem. Commun.*, 1990, **6**, 476.
16. Huybrechts D. R. C., Bruycker L. D. and Jacobs P. A., *Nature*, 1990, **345**, 240.
17. Na K., Jo C., Kim J., Cho K., Jung J., Seo Y., Messinger R. J., Chmelka B. F. and Ryoo R., *Science*, 2011, **333**, 328.
18. Roth W. J., Kresge C. T., Vartuli J. C., Leonowicz M. E., Fung A. S. and McCullen S. B., *Stud. Surf. Sci. Catal.*, 1995, **94**, 301.
19. Corma A., Fornes V., Pergher S. B., Maesen T. L. M. and Buglass J. G., *Nature*, 1998, **396**, 353.
20. Přech J., Eliášová P., Aldhayan D. and Kubů M., *Catal. Today*, 2014, **243**, 134.
21. Kim S.-Y., Ban H.-J. and Ahn W.-S., *Catal. Lett.*, 2007, **113**, 160.
22. Corma A., Díaz U., Fornés V., Jordá J. L., Domine M. and Rey F., *Chem. Commun.*, 1999 779.
23. Jin F., Chen S.-Y., Jang L.-Y., Lee J.-F. and Cheng S., *J. Catal.*, 2014, **319**, 247.
24. Ruan J. F., Wu P., Slater B. and Terasaki O., *Angew. Chem. Int. Edit.*, 2005, **44**, 6719.
25. Wu P., Tatsumi T., Komatsu T. and Yashima T., *J. Phys. Chem. B*, 2001, **105**, 2897.
26. Taramasso T., Perego G. and Notari B., ed. Snamprogetti S.P.A., US 4410501, 1983.
27. Zukal A. and Kubu M., *Dalton Transactions*, 2014, **43**, 10558.
28. Maheshwari S., Jordan E., Kumar S., Bates F. S., Penn R. L., Shantz D. F. and Tsapatsis M., *J. Am. Chem. Soc.*, 2008, **130**, 1507.
29. Roth W. J. and Dorset D. L., *Micropor. Mesopor. Mat*, 2011, **142**, 32.
30. Hutter R., Mallat T. and Baiker A., *J. Catal.*, 1995, **153**, 177.
31. Miller J. B., Johnston S. T. and Ko E. I., *J. Catal.*, 1994, **150**, 311.
32. Chen S.-Y., Tang C.-Y., Lee J.-F., Jang L.-Y., Tatsumi T. and Cheng S. F., *J. Mater. Chem.*, 2011, **21**, 2255.
33. Schwartz V., Mullins D. R., Yan W. F., Zhu H. G., Dai S. and Overbury S. H., *J. Phys. Chem. C*, 2007, **111**, 17322.
34. Farges F., Brown G. E., Jr., and Rehr J. J., *Phys. Rev. B*, 1997, **56**, 1809.
35. Fraile J. M., Garcia J. I., Mayoral J. A., Vispe E., Brown D. R. and Naderi M., *Chemical Communications*, 2001, **0**, 1510.
36. Wu P. and Tatsumi T., *J. Catal.*, 2001, **202**, 245
37. Wang L. L., Liu Y. M., Wang Y., Xie W., He M. Y. and Wu P., *Stud. Surf. Sci. Catal.*, 2008 **174**, 24.